Study of dynamic debris impact load on flexible debris-resisting barriers and the dynamic pressure coefficient

H.W.K. Lam[a], E.H.Y. Sze[a], E.K.L. Wong[a,*], S. Poudyal[b], C.W.W. Ng[b], S.L. Chan[c], C.E. Choi[d]

[a] Geotechnical Engineering Office, Civil Engineering and Development Department, Government of Hong Kong S.A.R., China (*Corresponding author eugeneklwong@cedd.gov.hk)

[b] Department of Civil and Environmental Engineering, Hong Kong University of Science and Technology, Hong Kong, China

[c] Department of Civil and Environmental Engineering, Hong Kong Polytechnic University, Hong Kong, China

[d] Department of Civil Engineering, University of Hong Kong, Hong Kong, China

Abstract

The use of steel flexible barriers to mitigate landslide risk on natural hillsides is becoming common in the last decade in Hong Kong. The current design approach for this kind of barrier structure involves the adoption of the hydrodynamic load model to predict dynamic impact forces, followed by non-linear structural analyses of flexible barriers using numerical programs based on the pseudo-static force method. From local design guidelines, the dynamic pressure coefficient, a critical input parameter in the hydrodynamic load model, is taken as 2.0. This empirically considers the effect of impacts from boulders up to 2.0 m in diameter. With a view to rationalising the design approach, a series of physical impact tests and numerical analyses was conducted to investigate the dynamic debris impact on flexible barriers and the resulting barrier response. The physical impact tests involved up to 9 m^3 of debris resisted by a 1.5 m high steel ring-net barrier. The tests were conducted in the 28 m long large-scale flume facility at the Kadoorie Centre in Hong Kong. Numerical modelling using computer programs LS-DYNA and NIDA-MNN was conducted to analyse the dynamic response of flexible barriers with different structural forms. The study aims to evaluate the dynamic pressure coefficient and to verify the current design approach based on the suggested dynamic pressure coefficient from this study. Results indicate that a dynamic pressure coefficient of 1.0 is in general appropriate for design purposes if the debris comprises primarily water and fine-grained particles.

Keywords: debris flow, flexible barrier, dynamic impact, physical tests, numerical modelling

1 Introduction

The impact of landslide debris on flexible barriers is a complex phenomenon. It is affected by multiple factors including turbulence in the flowing debris, energy dissipation within the debris during the impact process, and deformation of the flexible barrier and its various components. Researchers have attempted to study the behaviour of debris-barrier interaction using small-scale modelling of dry granular flow, e.g. Xiao et al. (2020); Tan et al. (2021); Zhang et al. (2021). Discrete element modelling is sometimes employed to simulate the behaviour of dry granular flows but is subject to difficulties including heavy computational demand when applied to field-scale problems or developing routine engineering designs.

Alternatively, larger-scale physical tests (Tan et al., 2020) or back analysis from field measurements obtained in instrumented full-scale barriers (Wendeler et al., 2019) have been attempted, supported by measurements of impact forces and simplified load models. With appropriate interpretation and due conservatism, these simplified approaches have the potential of being able to provide technical guidance for full-scale geotechnical design.

Flume facilities are commonly used by flexible barrier manufacturers to carry out debris impact tests to verify the performance of proprietary barrier products or to calibrate model parameters for specific numerical programs: e.g. DeNatale et al. (1999), Bugnion et al. (2012), WSL (2011).

There is a lack of established design methods for flexible barriers worldwide. In countries which have a long history of facing debris flow and rockfall hazards such as Switzerland and Italy, the design and manufacture of flexible barriers have been based on the energy approach, and more recently the force approach. The energy approach relies on the quantification of impact energy and selection of a barrier with an appropriate energy rating, usually proprietary products. On the other hand, under the force approach, components in a flexible barrier are explicitly designed based on structural analysis and member design. There is a need for a reliable and rational approach for the assessment of dynamic debris impact loads for barrier design. So far, less emphasis has been placed on the analysis of the dynamic pressure coefficient for flexible barriers under debris flow impact.

1.1 Design approach for flexible barriers in Hong Kong

In Hong Kong, flexible debris-resisting barriers are commonly used to resist debris from natural terrain landslides. Kwan and Cheung (2012) suggested to use the Energy Approach or Force Approach for the design of flexible debris-resisting barriers. In the Force Approach, the loading on flexible barriers involves the dynamic impact load as well as the static earth pressure arising from the debris deposited behind the barrier (e.g. Wendeler, 2008). Figure 1 shows the design impact scenario where the continuous impact of the debris flow is discretised into multiple loading steps or "surges" until the barrier is filled and further incoming debris overtops the barrier. This multiple surge load model is similar to that adopted by EOTA (2016). The dynamic impact load is assumed to be uniformly distributed across the width and depth of the moving debris and is assessed using the hydrodynamic equation as shown in Equation 1.

$$F = \alpha \rho v^2 h w \sin\theta \tag{1}$$

where

F = dynamic debris impact force

α = dynamic debris pressure coefficient

ρ = mass density of debris

v = impact velocity of debris

h = debris flow thickness

w = debris flow width

θ = inclination of dynamic debris impact force

Kwan and Cheung (2012) suggested to take the dynamic pressure coefficient (α) empirically as 2.0, which is deemed to cover the effects of impacts from boulders up to 2 m in diameter. The static load of deposited debris takes into account the self-weight of the moving debris above. The static earth pressure coefficient (K) is taken as 1.0. For a given design debris impact event, (i.e. flow volume, velocity, depth and width), both the dynamic impact load and static load are predicted. Based on these predicted loads, structural analyses of flexible barriers are conducted, which typically involve the use of structural analysis programs such as NIDA-MNN (Chan et al., 2012). The predicted loads are all taken as pseudo-static in each surge in the analysis. The structural analyses allow the prediction of cable reaction forces and the deformation of the flexible barrier. Further details on the structural modelling using NIDA-MNN are given in Section 4.

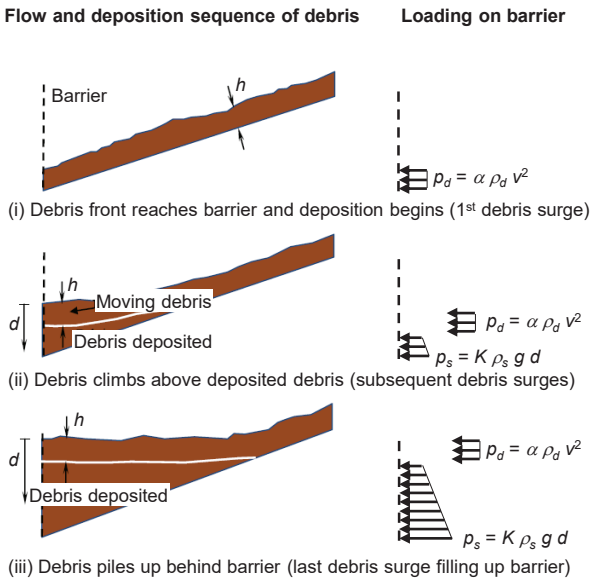

Figure 1. Design impact scenarios under Force Approach after Kwan and Cheung (2012)

1.2 Objectives of this study

The objective of the present study is to examine the value of the dynamic pressure coefficient, which is a critical input parameter in the hydrodynamic load model for predicting dynamic impact forces. This was achieved by a series of physical tests (see Section 2) as well as advanced numerical modelling using LS-DYNA (see Section 3). The physical tests involved large-scale physical flume experiments with up to 9 m^3 of debris impacting onto model barriers up to 1.5 m high (see Section 2). They were carried out in a controlled environment, where key critical parameters including the pre-impact flow conditions (viz. flow speed, depth and width) as well as the model barriers' cable loads and deflection profiles were measured or assessed. Based on field measurements, the dynamic pressure coefficients were back-calculated using Equation 1. In addition, advanced numerical modelling was performed using LS-DYNA to simulate two 400 m^3 debris flow events impacting onto a 16 m wide barrier. Although the debris flow events were hypothetical, the model parameters used in the simulation had been calibrated against documented large-scale physical tests reported in the literature. The LS-DYNA modelling allows coupled analyses that simulate both the debris flow process and the impact process in a computational run. It computes the pre-impact flow conditions of the debris as well as the model barriers' cable loads

and deflection, etc., for a given debris volume and geometry of flume setting. These numerical outputs also allow an interpretation of the dynamic pressure coefficients. Results for the physical tests and numerical modelling are given in Sections 2 and 3 respectively.

In the second part of this paper, the design approach (as briefly discussed in Section 1.1) is verified by NIDA-MNN simulation of two real impact scenarios at 1:1 scale based on the multiple surge load model in Figure 1, and the suggested dynamic pressure coefficient from this study. Comparison of the numerical predictions, in terms of the cable load and barrier deformation, against the field measurements is made. Results are reported in Section 4.

A review of the design of some 60 recent flexible debris-resisting barriers under the Landslip Prevention and Mitigation Programme in Hong Kong indicated that the majority (85%) of the engineering designs involved a total debris volume (debris source plus entrainment) of 200 m^3 or less. Besides, the design flow depth was relatively shallow: about 58% of cases involving a flow depth of 0.5 m or below. For debris flows involving such shallow flow depth, the probability of large boulders being transported may not be high. The finding of this study is applicable to landslide debris that primarily comprises a mixture of water and fine-grained particles without boulders.

This study documents a systematic approach for establishing an appropriate design value of the dynamic pressure coefficient for the engineering design of debris-resisting flexible barriers generally. This was made possible by results of physical impact tests with instrumented flexible barriers using one of the largest geotechnical flume facilities available, corroborated by numerical simulations of typical full-scale flexible barriers.

2 Physical impact tests at Kadoorie Centre, Hong Kong

2.1 General

The dynamic impact on a flexible barrier is highly complex and is strongly affected by debris-barrier interaction. Both the debris flow characteristics as well as the flexibility of the barrier structures are the important factors. The flexibility of a barrier is controlled by its structural form and overall layout, the mechanical properties of constituent components (including the ring-net, posts, cables, brake elements, etc.) and their interactions. There is a general lack of established methods or scaling laws to predict the dynamic impact load on a flexible barrier based on down-scaled barrier models. Therefore, in this study, large-scale impact tests with debris flows up to 9 m^3 were carried out.

The tests were conducted between 2019 and 2020 using the large-scale flume facility at the Kadoorie Centre in Hong Kong (Ng and Choi, 2019, 2020). The flume is one of the largest flumes of its kind in the world for simulating debris flow under a controlled setting. Large-scale flume facilities are typically purpose-built for investigating specific aspects of physical phenomena. The 95 m long USGS debris flow flume (Iverson, 1997) was built to study debris flow dynamics. Bugnion et al. (2012) studied debris flow impact against flexible barriers in a 50 m long natural rock slope. Won et al. (2016) carried out debris flow erosion experiments in an 850 m channel to characterize erosion deposition patterns with LiDAR. However, it is difficult to replicate experiments in natural channels and slopes due to inherent variability of the sites. To carry out repeatable debris flow impact experiments in a controlled setting, a large-scale debris flow flume was purposefully built in Hong Kong, with high quality instrumentation including pressure cells developed in-house for

measuring flow characteristics and the transient response of flexible barriers throughout the impact process.

Details of the flume facility, setup, model barriers, debris mix and test programme are discussed in the following subsections.

2.2 Flume facility and test setup

The flume established at the Kadoorie Centre is about 28 m long, 2 m wide and 1 m deep (see Fig. 2). It comprises three key components, including a storage tank upstream, a transportation channel, and a deposition zone at its downstream end.

The storage tank has a capacity of about 10 m^3, with a gradient of 30 ° at the base to facilitate initiation of debris flows. A double-door gate which is water-tight around its edges is used to retain debris material inside the storage container. The doors are secured by a mechanical arm controlled by an electric motor.

The transportation channel is rectangular in cross-section and inclined at 20 °. Its length is about 15 m. One of the side walls is made of transparent acrylic, which allows the observation of flow behaviour. The other side wall and the flume base are made of steel plates.

The deposition zone is 2 m wide and 8 m long, located at the outlet of the transportation channel. It is founded on a 5 m wide and 8 m long level concrete pad.

Figure 2. Flume facility (with Barrier 2 installed)

2.3 Model barriers

Four tests were conducted involving two types of flexible barriers of different sizes (viz. Barrier 1 and Barrier 2).

Barrier 1 was used in Test 1 (see Fig. 3). It was installed 13.5 m from the gate in the transportation channel inside the flume. The barrier was formed by a 100 mm diameter ring net made of 4 windings of 2 mm diameter steel wire. The ring net panel was 0.8 m high and 2 m wide, and supported by two longitudinal load-bearing cables at the top and bottom. These two cables were 12 mm in diameter, each connected to two brake elements (located at either end) and

anchored to the sides of the flume. Brake elements are important components in a flexible barrier, used to attenuate cable loads under dynamic impacts. In this barrier model, the brake elements were developed in-house at the Hong Kong University of Science and Technology (HKUST) (Ng et al., 2016). The force-elongation curve of the brake elements is given in Figure 4, which was derived following the test procedure set out in ETAG 27 (EOTA, 2013). A layer of secondary mesh with 25 mm diameter opening was provided at the upstream side of the ring net to help retain the soil debris with the aim of maximising the debris impact load. The barrier was installed orthogonal to the base of the flume, i.e. tilting downslope by about 20 ° to the vertical.

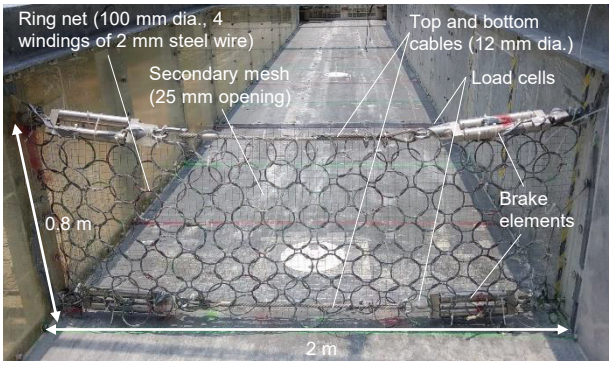

Figure 3. Barrier 1

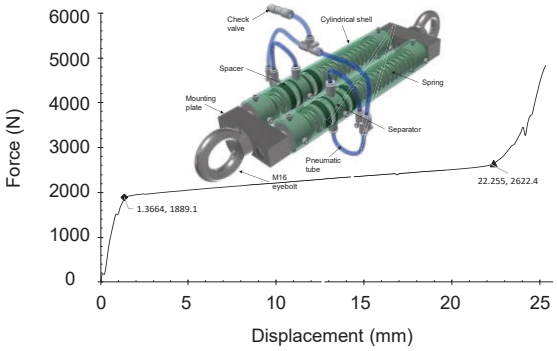

Figure 4. Characteristics of brake element installed in Barrier 1 (Test 1) (Ng et al., 2021a)

Barrier 2 was used in Test 2 (also referred to as Test BDW25) as shown in Figure 5 and was placed at the deposition zone. It was formed by a 200 mm diameter ring net made of 7 windings of 3 mm diameter steel wire. The ring net panel was 1.5 m high and 4 m wide, and supported by three longitudinal cables at the top, middle and bottom. These cables were 16 mm in diameter, each of which was connected to a single brake element at one end of the cable in a staggered manner (see Fig. 5). These cables were anchored to a steel portal frame. A secondary mesh with 6 mm diameter opening was provided at the upstream side of the ring net. The barrier was installed orthogonal to the base of the deposition zone (i.e. vertical). The model of the brake elements used was the Trumer AVT Phx 60/30-1.5. An image of the brake element and its loading response following the test procedure set out in ETAG 27 (EOTA, 2013) are presented in Figure 6. The brake element model has an activation force of about 48 kN.

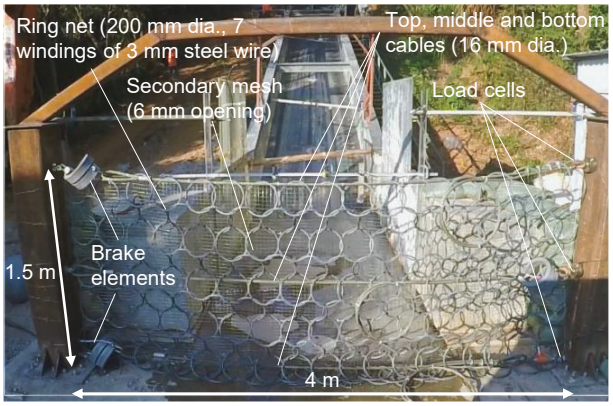

Figure 5. Barrier 2 (Test 2)

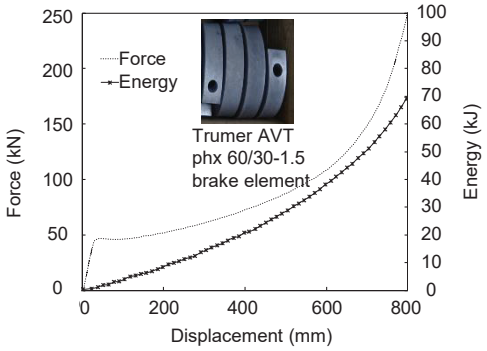

Figure 6. Brake element and characteristic curve used in Tests 2 and 3

For Test 3 (also referred to as Test NMBDW30), Barrier 2 was modified by removing the middle cable. For Test 4 (also referred to as Test NBDW40), Barrier 2 was modified by removing all brake elements (Table 3).

In all tests, any mobilised brake elements and damaged secondary meshes were replaced before conducting the subsequent test.

2.4 Instrumentation system

The instrumentation used in the tests is summarised in Figures 7 and 8. Two high-speed cameras, along with a regular camera, were installed to capture the impact process and to collect flow data such as velocity and depth of the debris flows. Laser sensors and ultrasound sensors were installed at various locations of the flume for the measurement of flow depth. A load cell was installed in each cable for cable load measurement. Specifications of the instruments are given in Table 1. These instruments were calibrated before use.

Table 1. Details of instruments

Instruments	Measurable range	Frequency	Accuracy	Key purpose
Laser sensor	< 1 m	2 kHz	$\pm$ 0.5%	To capture flow depth
Ultrasound sensor	< 2 m	2 kHz	$\pm$ 0.1%	To capture flow depth
Basal load cell at deposition zone	< 1.1 kN	2 kHz	$\pm$ 0.02%	To capture vertical pressure of debris flow
Load cells for cable load	$<$ 50-100 kN	2 kHz	$\pm$ 0.05%	To capture impact force of debris
High-speed camera (2336 $\times$ 1728 pixels)	-	560 fps	-	To capture kinematics of flow-barrier interactions (e.g. debris flow velocity and flow depth)
Camera (1980 $\times$ 1080 pixels)	-	60-120 fps	-	To capture kinematics of flow-barrier interactions (e.g. debris flow velocity and flow depth)
Unmanned aerial vehicles (1980 $\times$ 1080 pixels)	-	30-60 fps	-	To capture kinematics of flow-barrier interactions (e.g. debris flow velocity and flow depth)

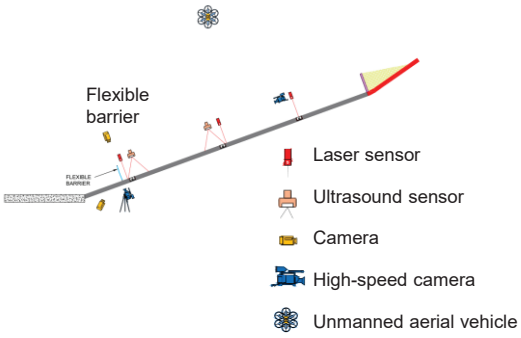

Figure 7. Instrumentation in Test 1

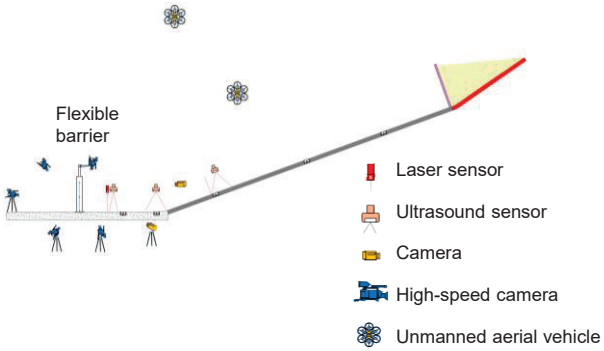

Figure 8. Instrumentation in Tests 2 to 4

2.5 Debris material

In this study, a debris mix with 25 to 40% of water by volume was adopted. Details of the solid content of the debris mixture are given in Table 2. Regardless of the water content used, the composition of the solid content was kept constant. The d_{95} particle size was 25 mm. A similar debris mix was used for the testing of rigid barriers and the details of derivation of the mix composition can be found in Lam and Wong (2021). Debris material was mechanically mixed by a concrete truck mixer to ensure consistency of material before being transported to the storage tank of the flume via a chute system.

Table 2. Debris flow compositions

Debris mixture with 40% water content by volume					
Material	Gravel	Sand	Silt/Clay	Total solids (kg)	Water (40%)
Mass (kg)	558	957	40.6		
Particle size (mm)	35	2.00	0.06	1555.6	406
Cumulative PSD	100%	64%	3%		
Total mass fraction	0.25	0.49	0.02	0.79	0.21
Debris density (kg/m^3)				2000	
Debris mixture with 30% water content by volume					
Material	Gravel	Sand	Silt/Clay	Total solids (kg)	Water (40%)
Mass (kg)	655	1127	52		
Particle size (mm)	35	2.00	0.06	1834	300
Cumulative PSD	100%	64%	3%		
Total mass fraction	0.31	0.53	0.02	0.86	0.14
Debris density (kg/m^3)				2100	
Debris mixture with 25% water content by volume					
Material	Gravel	Sand	Silt/Clay	Total solids (kg)	Water (40%)
Mass (kg)	703	1210	52		
Particle size (mm)	35	2.00	0.06	1965	250
Cumulative PSD	100%	64%	3%		
Total mass fraction	0.32	0.55	0.02	0.89	0.11
Debris density (kg/m^3)				2200	

Table 3. Test plan

Test No.	Model barrier	Debris source volume (m^3)	Water content of debris mix
1	Barrier 1	2.5	40%
2 (BDW25)	Barrier 2	9	25%
3 (NMBDW30)	Modified Barrier 2 (no middle cable)	9	30%
4 (NBDW40)	Modified Barrier 2 (no brake elements)	9	40%

2.6 Test plan

Four tests were carried out as summarised in Table 3. As discussed in Section 1, the key objective of this series of large-scale flume tests is to study dynamic debris pressure coefficient (α). For each test, the storage tank was first filled with a designated volume of debris mix. The debris material was then released from the storage tank, through a mechanical gate, to initiate a debris flow. The debris material would flow along the transportation channel and impact onto the model barrier downstream. The flow characteristics, such as flow depth, flow velocity, etc. and the response of the barrier under debris impact were captured.

2.7 Test results

2.7.1 Kinematics of debris flow impact on model flexible barrier

Figure 9 shows the impact kinematics in Test 1 as captured by the high speed camera and is accompanied by a qualitative sketch of the impact process observed. When the debris hit the model barrier (at $t = 6.3$ s in Fig. 9), the barrier began to deform along the direction of impact, and it was evident that some debris leaked through the opening of the netting, while some debris was retained. When the impact process proceeded (from $t = 6.3$ to 7.1 s), the continuous inflow of debris ran up the deformed barrier in a curved trajectory, slightly deflected backwards in the air, and then rolled back onto the

Table 4. Summary of field tests on dynamic load

Test no.	Flow velocity (m/s)	Flow depth (mm)	Flow density (kg/m^3)	Cable	Peak cable deflection at anchor (°)	Peak cable tension T (kN)	Component N of tension along flow (kN)	Resultant force $\Sigma 2N$ (kN)	Back calculated α	Filling height* (m)
1	4.5-5.2	60	2000	Top	12	4.1	0.86	4.64	0.71-0.90	0.7
				Bottom	12	7.0	1.46			
2 (BDW25)	7.6-8.5	350-380	2200	Top	4.4	17.47	1.34	53.97	0.45-0.61	0.5
				Middle	17	40.41	11.81			
				Bottom	17	47.33	13.83			
3 (NMBDW30)	9.1	200-300	2100	Top	16	45.20	12.46	52.78	0.51-0.76	0.6
				Bottom	16	50.53	13.93			
4 (NBDW40)	9.2	190-200	2000	Top	3	23.89	1.25	50.74	0.75-0.78	0.5
				Middle	10	69.03	11.99			
				Bottom	10	69.85	12.13			

* Measured perpendicular to flume base

Table 5. Net movement and brake mobilisation

Test no.	Max. net deflection (forward bulging)	Brake element mobilisation	Residual height
1	240 mm	Brakes at top and bottom cables fully mobilised	0.70 m
2 (BDW25)	520 mm	Brakes at middle and bottom cables partially mobilised	1.35 m
3 (NMBDW30)	1040 mm	Brakes at top and bottom cables partially mobilised	1.10 m
4 (NBDW40)	480 mm	N/A (No brakes used)	1.40 m

flume, interacting with the subsequent inflow of the debris. Significant turbulence of the debris flow occurred behind the barrier net (at $t = 7.9$ s). The inflow of debris subsided and a more or less levelled deposition profile was observed towards the end of the test (see $t = 10$ s). The filling height in each test is shown in Table 4

Comparing the results of Tests 2 to 4 which involved the same test volume of 9 m^3, it was observed that the increasing water content of the debris mix tends to result in an increase of the debris flow velocity and a decrease of the flow depth (2nd and 3rd columns in Table 4). Also, more debris (i.e. the fluid portion) would leak through the net opening if its water content was higher. The deflection of the barrier net after the impact tests and other key observations are summarised in Table 5 and Figure 10.

2.7.2 Interpretation of dynamic debris pressure coefficient α

The interpretation of dynamic debris pressure coefficient (α) requires various input parameters including impact force, flow depth, flow velocity, width of impact, debris density and impact angle, based on Equation 1.

Impact force

The impact force (F) refers to the debris impact force acting in the flow direction, i.e. normal to the net panel. It can be assessed based on the measured cable loads as well as the cable deflections at the supports, following the same approach adopted by other researchers (e.g. Song et al., 2018). The measured cable loads are shown in Figure 10. The measurements indicate that there was a dynamic load at the very beginning (about 1 s from the time when the cable load first became mobilised). This was particularly obvious in Tests 2 to 4 where, at steady state, the cable forces in general

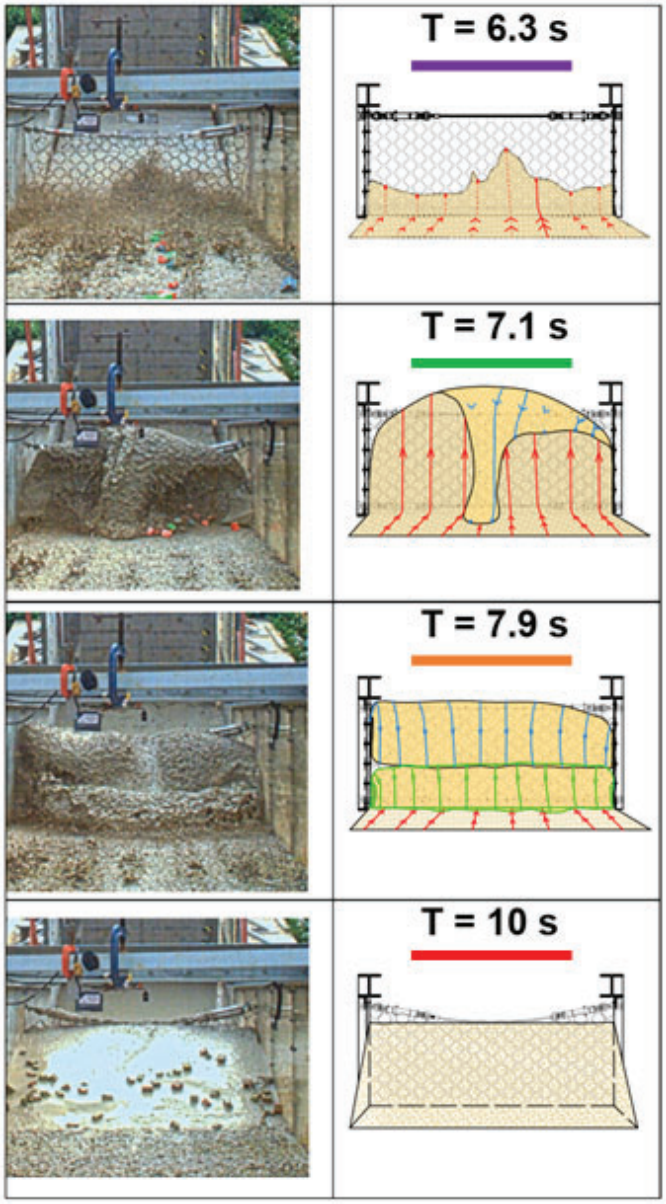

Figure 9. Debris impact mechanism for Test 1

dropped to less than half the peak values during impact.

To determine the impact force exerted by the debris flow onto the barrier, the cable load has to be resolved into the force component normal to the impact face of the barrier. As such, the cable deflections at the support has to be analysed. Details of the procedure are presented in Appendix A. The cable deflection angle at the anchors for the top cable and middle cable (if any) were tracked using the PROTRACTOR tool available in the Tracker Video Analysis software (Brown, 2016). The video for analyses was captured from the top view and was recorded at a frame rate of 120 fps (Δt = 0.00833 s). The image used were corrected for radial distortion errors. For the bottom cable, as it was visually obscured by the net from the top view, it is assumed to follow deflected profile of the middle cable for Tests 2 and 4 and that of the top cable for Test 3, given that the measured cable load in bottom cable was very close (average $< 10\%$ difference) to that of the middle cable for Tests 2 and 4 and that of the top cable for Test 3. The summary of the cable deflection for each cable for the tests are given in Table 4.

The cable load should in theory also be adjusted due to the deflection of the cable projected on the vertical plane (i.e. deflection of cable from the front view). From field observations, the deflection angle in the vertical plane was generally about 20 ° or lower. Such deflection has no significant bearing on the impact force interpreted (cos 20 ° = 0.94, i.e. about 1.0) or the α value, and this was conservatively neglected in the analyses in Table 4.

From the perspective of interpreting the α value, the peak cable load during the period of dynamic impact (i.e. initial first two seconds of the impact for Test 1 and initial first second of the impact for Tests 2 to 4 from Fig. 10) was used for the interpretation of the α value. This ignores any possible effects of static pressure of the deposited debris acting on the barrier, and would err on the conservative side.

Comparing the cable loads for Tests 2 to 4, it is noted that in Tests 2 and 3 which involved barriers with brake elements, the cable loads were capped by the activation force of the brake element (about 48 kN), while the cable load in Test 4 for a barrier without brakes could reach about 70 kN. This shows the function of brake elements in attenuating cable loads.

Flow depth

The debris flow depth at a short distance (about 1.5 m to 3 m) upstream of the model barriers was analysed based on records of laser sensors and ultrasound sensors, corroborated by the depth observed from high-speed cameras capturing the side view of the flume through the transparent wall. In some tests, the reading from laser sensor and ultrasound was either missing (due to the damage of the instruments by debris reflected from the barrier), or showed aberrant readings such as spurious spikes. The measured data from ultrasound and laser sensors were filtered using a low pass filter with cut-off frequency of 300 Hz to remove spurious high frequency noise. Nonetheless, some high frequency artefacts of around 200 Hz persists in the filtered signal most likely due to the capture of minor splashing of the debris instead of the actual flow depth. In these cases, the flow depth was based on the analyses of high speed videos from the side of the flume. The results of the flow depth are given in Table 4.

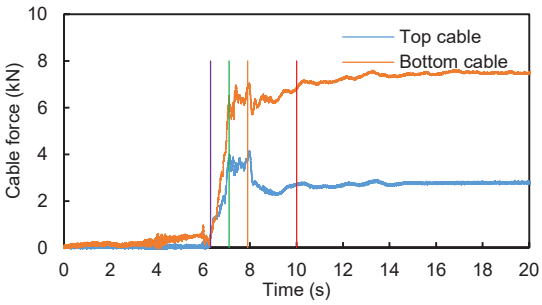

Refer to Fig. 9 for debris impact mechanism at specified time instants

(a) Test 1

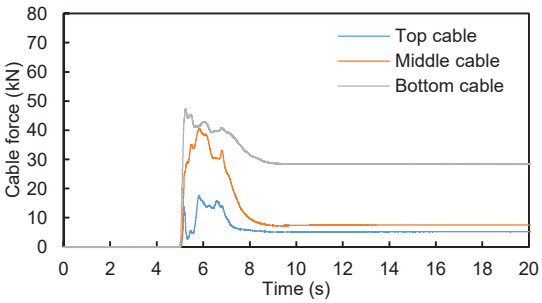

(b) Test 2

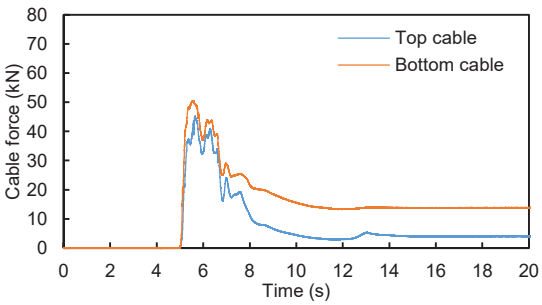

(c) Test 3

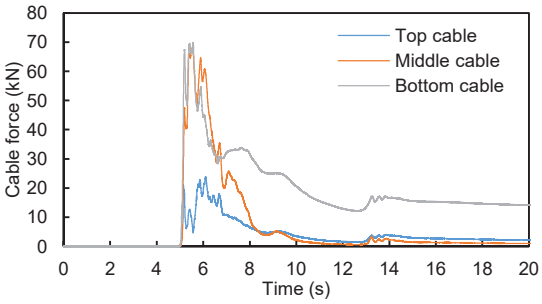

(d) Test 4

Figure 10. Cable force time histories and general view of barrier at maximum net deflection

Flow velocity

The debris flow velocity at about 1.5 m to 3 m upstream of the barrier was analysed by Tracker Video Analysis (Brown, 2016). At least 3 points were taken for tracking down the velocity in each section (i.e. a point in the middle plus two points near side walls). Flow velocity was deduced based on the records from UAV, cameras, and high-speed cameras. The frontal flow velocity was checked against the velocity assessed based on the measured time elapsed between the arrival of the debris to two instruments at the deposition zone and the distance between the instruments. Video analyses indicated that the frontal part of the flow, that is within the first second of the flow body that contributed to the peak impact load, did not show notable reduction in the flow velocity for Tests 3 and 4 and the frontal flow velocity was adopted for analysing the α value. For other tests, a range of flow velocity from the highest at the flow front to a lower velocity in the trailing flow (still within the first second of the flow body from the frontal) was considered to interpret the debris pressure coefficient, as shown in Table 4.

Other parameters

The width of debris impact was taken as the channel width which is 2.0 m for all tests. Debris density was taken as the initial debris density estimated based on the debris mix proportion, which ranges from about 2,000 kg/m^3 to 2,200 kg/m^3 for the tests (see Table 2). The impact angle was taken as 90 ° based on field observation.

Results of α values

Based on Equation 1, the dynamic debris pressure coefficient α was found to range from 0.45 to 0.90 as shown in Table 4. It appears that Test 4 (NBDW40) and Test 1, which refer respectively to the test without brake elements and the test with brake elements having been fully mobilised, tend to result in a slightly higher α value of 0.8 to 0.9, but still below unity.

Compared to the experimental study on rigid barriers (Lam and Wong, 2021), in which the dynamic debris pressure coefficient was found to range from 0.73 to 1.01, the α value for flexible barrier is comparable but slightly lower. Based on flume tests at different scales, Ng et al. (2021a,b) have recommended similar α values for the design of rigid and flexible barriers.

3 Numerical analyses using LS-DYNA to simulate large-scale events to examine dynamic pressure coefficient

In this study, advanced numerical analyses were conducted to simulate debris flow impacts onto flexible barriers using the three-dimensional finite-element computer program LS-DYNA. The numerical models allow the simulation of both the debris flow and impact processes. The replication of the flume test using LS-DYNA has been carried out and reported in Lam et al. (2022). Reasonable agreement has been achieved between simulated and measured cable forces and net

Table 6. Material model and input parameters in LS-DYNA simulations

Materials	Material model	Input parameters	Remarks
Debris	MAT_SOIL_AND_FOAM	Density = 2200 kg/m^3 Shear modulus = 500 kPa Bulk modulus = 1000 kPa Internal friction angle = 15° Basal friction alge = 12°	Calibrated parameters by Kwan et al. (2019)
Steel net	MAT_HYSTERETIC_BEAM	Density = 7800 kg/m^3 Young's modulus = 200 GPa Poisson's ratio = 0.3	Typical material properties
Cable	MAT_ELASTIC	Density = 7800 kg/m^3 Young's modulus = 100 GPa Poisson's ratio = 0.3	Typical material properties
Brake element	MAT_INELASTIC_SPRING_DISCRETE_BEAM	Force-elongation curve: x_1 = 0.05 m, y_1 = 100 kN x_2 = 0.45 m, y_2 = 113 kN x_3 = 1.05 m, y_3 = 285 kN	Typical values of proprietary brake elements

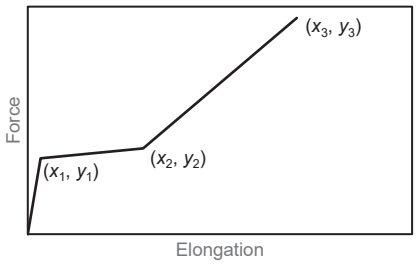

movements.

Two numerical simulations were conducted. Simulation 1 involved a debris source volume of 400 m^3, flowing along a 10 m wide, 15 ° steep channel, and impacting onto a 6 m high trapezoidal side-anchored barrier as shown in Figure 11. Brake elements were provided in each of the cable elements. The initial flow velocity was about 12 m/s, while the impact velocity when reaching the barrier was about 8 m/s to 11 m/s. The flow density was taken as 2,200 kg/m^3. The impact angle was normal to the barrier. Simulation 2 was the same as Simulation 1, except that no brake elements was provided for all cables. Figure 12 shows the numerical runs for Simulations 1 and 2.

Arbitrary Lagrangian-Eulerian (ALE) technique was adopted to simulate the landslide debris as a continuum material, where the internal rheology was characterised using the Drucker-Prager yield criterion. The internal friction angle and basal friction angle for the ALE material were assumed to be 15 ° and 12 ° respectively with reference to Koo (2017), which were also calibrated against published impact case histories (Kwan et al., 2019). These case histories involved debris flow without large boulders. The modelling technique and validation of the numerical models are also detailed in Kwan et al. (2019). The material models and associated input parameters for debris and different components of the flexible barriers are summarised in Table 6.

To simulate the effects of the secondary mesh, a virtual impervious membrane was applied to the surface of the nets. The membrane was modelled as "null" shell elements acting as an invisible elastic layer so that the debris could not penetrate through the net. The membrane itself has neither stiffness nor strength and is connected only to the nets. Therefore when the debris hits the membrane, all forces would be transmitted to the nets and other components.

The contact between the soil (modelled as ALE material) and the flexible barrier (modelled as impervious null shell elements) was handled using penalty coupling method (Aquelet et al., 2006; Olovsson and Souli, 2000). This method

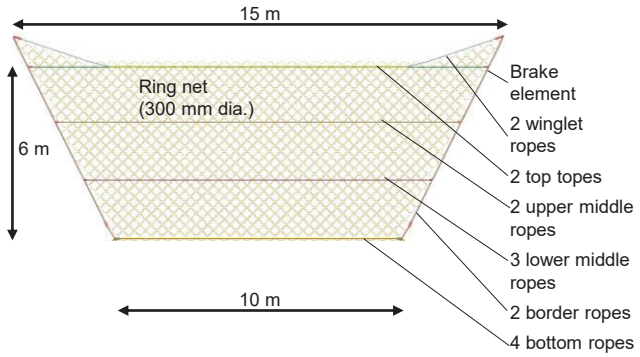

Figure 11. Side-anchored Barrier model adopted in Simulation 1

searches for interactions between the ALE material and the shell elements, and then tracks the independent motions of the contacting elements over a small time step. Any penetration of the ALE material into the shell elements induces a normal interface reaction force, which is distributed evenly to both elements. The magnitude of the force is proportional to the penetration and is calculated using an interface spring stiffness, which is governed by the Young's moduli of the ALE material and the shell elements. Details can be found in Kwan et al. (2019). Similar LS-DYNA modelling techniques for flexible barriers under impact have also been adopted by other geotechnical practitioners (Koo et al., 2017; Cheung et al., 2018; Kwan et al., 2021).

For these two simulations, the numerical outputs regarding the pre-impact flow conditions (e.g. flow depth, flow width and flow velocity) and barrier response (e.g. peak cable load and deflection of cables at anchorage locations) were analysed in the same manner as for the physical tests in Section 2. Using Equation 1, α was found to be 0.56 and 0.99 respectively for Simulation 1 and 2 (see Table 7). These values are consistent with the findings from the physical impact tests reported in Section 2 and Ng et al. (2021a,b) in a sense that the α values are generally less than unity, and the absence of brake elements tends to give rise to a higher α value. For the sake of conservatism, an upper bound value of 1.0 is suggested for α, which was used in the NIDA-MNN modelling as described in Section 4.

Table 7. Summary of LS-DYNA simulations

No.	Any brake elements used	Debris impact velocity (m/s)	Debris flow thickness (m)	Peak impact force (kN)	α
1	Yes	8-10	2-3	2770-3661	0.56-0.61
2	No			3180-4186	0.61-0.99

4 Numerical prediction of barrier response using NIDA-MNN using force approach

As mentioned in Section 1, the objective of the present study includes the verification of the design approach for flexible barriers adopted in Hong Kong. This was done via NIDA-MNN simulation of real impact scenarios using model barriers at 1:1 scale based on the multiple surge load model (Fig. 1), and using the suggested dynamic pressure coefficient from this study. NIDA-MNN is a finite element design tool commonly used in Hong Kong for the structural design of flexible barriers (Sze et al., 2018). This is followed by a comparison between the numerical predictions, in terms of the cable loads and barrier deformation, and field measurements.

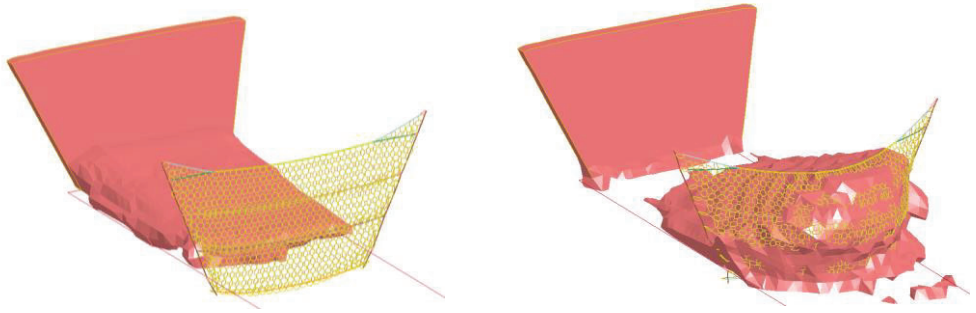

(a) Simulation 1 (with brake elements) (Left: T = 1.2 s, Right: T = 4.8 s)

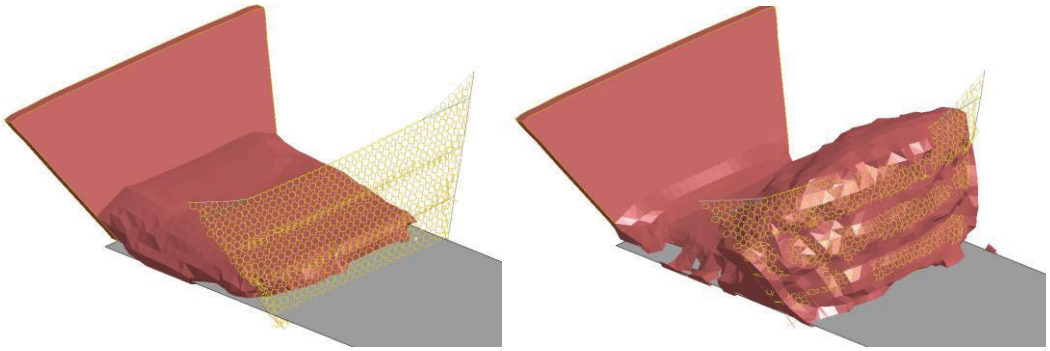

(b) Simulation 2 (without brake elements) (Left: T = 1.2 s, Right: T = 4.5 s)

Figure 12. LS-DYNA simulation for 400 m^3 debris flow impact

In this part of the study, selected case histories have been analysed using NIDA-MNN. This program simulates the nonlinear structural behaviour of a flexible barrier under loading. The program incorporates nonlinear elements to model brake elements, circular net rings, as well as sliding elements to simulate the contact between net elements and cables. Further details about the modelling technique and validation of the numerical models are discussed in Chan et al. (2012).

A thorough literature review has been conducted to take stock of documented large-scale debris impact tests on flexible barriers (> 10 m^3) carried out around the world (DeNatale et al., 1999; Wendeler et al., 2008b; WSL, 2011; Bugnion et al., 2012; Ferrero et al., 2015). Most of them were initiated by flexible barrier manufacturers, and not all data from these tests were available. Among these impact tests, two cases were selected for more in-depth analyses where relatively comprehensive test details were available: Case 1 at Illgraben by Wendeler et al. (2008a), which involved a 4 m high side-anchored barrier, and Case 2 at Veltheim by WSL (2011), which involved a 3.5 m high post-supported barrier. A summary is presented in Appendix B.

The simulation involved the load model (Fig. 1) used in the Force Approach (Kwan and Cheung, 2012), with an α value of 1.0. The barrier's response from the numerical simulation, in terms of peak cable force and deformation, was then compared against field measurements.

In these simulations, the frontal impact velocity is based on field measurements, whereas for the impact velocity in subsequent loading stages, account was taken of the velocity reduction as recommended by GEO (2015). The static earth pressure coefficient K (see Fig. 1) was taken as 1.0. The structural configuration of the flexible barrier was explicitly modelled. The cable force and the deformation of the barriers based on the above approach were used to compare with field measurements. Details of the simulations, including the layout of the model barriers, properties of their components, input of loads etc. for the two cases are given in Appendix B.

Table 8. Comparison of numerical simulation (NIDA-MNN) and field measurements for Case 1 – Illgraben site

Peak cable force (kN)	Prediction using force approach ($\alpha = 1, K = 1$)	Field measurement	Difference
Top rope	154	150	2.7%
Bottom rope	251	240	4.6%
Winglet rope	167	150	11.3%
Deformation of barrier	**Prediction using force approach ($\alpha = 1, K = 1$)**	**Field measurement**	**Difference**
Deflection (forward bulging) (m)	3.56	2.5	42.4%

The results of the simulations for the two cases are shown in Table 8, Table 9 and Figure 13. It is observed that the cable load and the deformation of the barrier are comparable to or, in some case, higher than from field tests. This suggests that the design approach described in Section 1.2, along with the suggested α value of 1.0 could give rise to a comparable and generally conservative prediction of cable load and deformation of flexible barriers under debris impact for the two cases considered.

From Tables 4 and 7, it is known that the dynamic pressure coefficient could be as low as 0.45 when debris-barrier interaction is considered. Hence it is reasonable for the simulated barrier deformations to exceed those measured in the

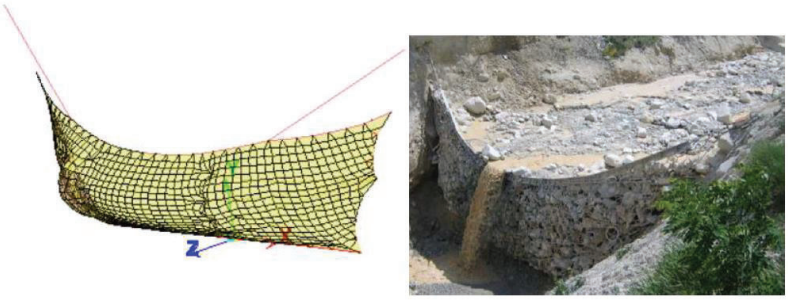

(a) Case 1

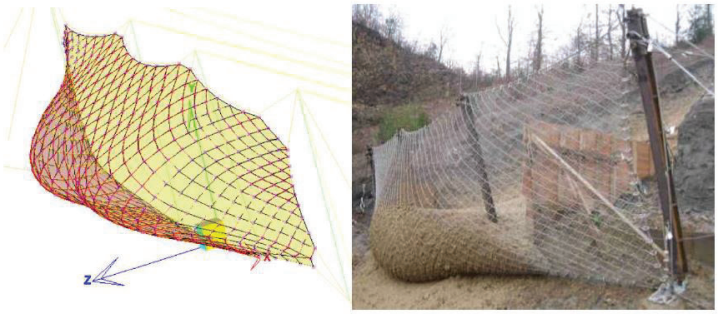

(b) Case 2

Figure 13. Comparison of deformed shapes of barriers between numerical models and field tests

field if a simplified uncoupled load model (i.e. Fig. 1) is used in the analysis with an upper-bound value of $\alpha = 1.0$.

In Case 2, the bottom cable force from the simulation is much higher than from field measurements, and this suggests that the dynamic load applied (based on $\alpha = 1.0$) in the first surge at the bottom area of the net could be on the conservative side.

Table 9. Comparison of numerical simulation (NIDA-MNN) and field measurements for Case 2 – Veltheim site

Peak cable force (kN)	Prediction using force approach ($\alpha = 1, K = 1$)	Field measurement	Difference
Top rope	85	84	1.2%
Bottom rope	203	82	148%
Winglet rope	63	50	26%
Deformation of barrier	**Prediction using force approach ($\alpha = 1, K = 1$)**	**Field measurement**	**Difference**
Deflection (forward bulging) (m)	2.35	2	17.5%

5 Discussion on dynamic debris pressure coefficient and way forward

From the physical impact tests discussed in Section 2 as well as the numerical analyses in Section 3, the dynamic impact force and the dynamic pressure coefficient α on flexible barriers due to debris impact have been examined. In all cases, the α value is consistently below unity . This α value is generally consistent with suggested values in international guidelines or literature. For example, Wendeler et al. (2008a) suggested that for debris flow involving a fluid event (debris density 1,900 kg/m^3), an α of 0.7 can be adopted. Volkwein (2014) also recommended an α of 0.7 to 1.0 for debris with a density

of 1,600 kg/m^3 to 2,000 kg/m^3 for debris without boulders, and in which case the effects of impacting blocks that may be carried along with the flow must be considered separately. Volkwein (2014) further suggested that an assessment of the impact of large individual blocks can be omitted if α was set as 2.0, but the limiting size of the boulders and the impact velocity in such cases was not clearly described.

The observed α value from this study does not apply to debris flows containing large boulders. When dealing with this type of debris flow material, the continuum method (e.g. ALE in LS-DYNA) has the limitation of not being able to model phase separation or the impact from boulders which is discrete in nature. In this regard, explicit modelling of individual discrete boulders, coupled with ALE material, may be considered in LS-DYNA. More study in this regard is needed. Alternatively, CFD-DEM coupled approaches can also be considered.

The current practice in Hong Kong adopts an α value of 2.0, which takes into account the effects of impacts from boulders up to 2 m in diameter. Based on the current study, as well as the available international guidelines and literature, it is considered more reasonable for designers to adopt a lower α value of 1.0 if the debris comprises primarily water and fine-grained particles without boulders or if the designers opt for independent measures (e.g. baffles or in-situ stabilisation) to account for boulders.

The current study does not examine the effect of boulders due to the relatively small scale of the flume facility at the Kadoorie Centre in Hong Kong, and there are very few reported cases of debris flows mixed with large boulders.

6 Summary and recommendations

Various studies to investigate dynamic debris impact on flexible barriers have recently been completed in Hong Kong. Based on large-scale physical tests and numerical analyses, a dynamic pressure coefficient of 1.0 is suggested if the debris comprises primarily a mixture of water and fine-grained particles without boulders or if independent measures such as baffles are provided to trap boulders. This coefficient can be used in the hydrodynamic equation for predicting debris impact loads in routine design show that the α value was consistently less than unity for dynamic soil debris impact on flexible barriers.

This study also shows that the use of pseudo-static force analysis using NIDA-MNN based on the load model considered (Fig. 1, along with a dynamic pressure coefficient of 1.0, is generally conservative.

Appendix A

Interpretation of α value from cable load measurements

In this appendix, the interpretation of the α value is illustrated using results from Test 1 using the hydrodynamic equation (Eq. 1). The debris impact force F was taken as the total of reaction forces at the four supports of top and bottom cables. The total reaction force is summation of components of the cable reaction force normal to the barrier net. This component of the reaction force depends on the load measured at the top and bottom cables, together with the deflection angle ψ of the cables at the supports (Fig. A.1). The time histories of the cable forces have been presented in Figure 10. The time history of the cable deflection angle for Test 1 is shown in Figure A.2.

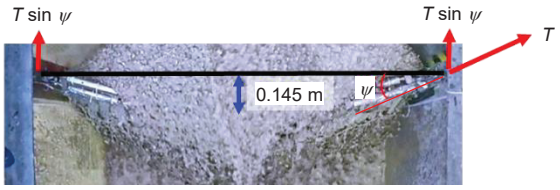

Figure A.1. View of debris impact from top showing deflection angle ψ

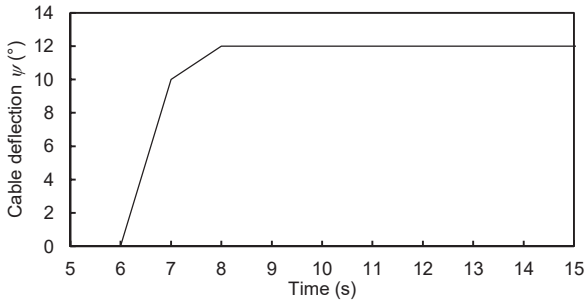

Figure A.2. Deflection angle time history

The deflection angle of the bottom cable was obscured by the net and debris. To assess the deflected profile of the bottom cable, the total length of the deflected bottom cable was assessed. The total length refers to the summation of the length of wire rope and the lengths of the two brake elements connected to the wire rope. From field measurements, the bottom cable measured a peak load of about 7 kN. Therefore the total length of the deflected bottom cable under dynamic load was assessed to be 3 mm (due to elastic extension of wire rope, with a cable length of 2 m, cross-sectional area of 55 mm^2, and Young's modulus of 96 GPa), plus 50 mm due to elongation of two brake elements from the load displacement curve (Fig. 4), plus the original length of 2.0 m, i.e. 2.053 m. A similar approach gives 2.052 m for the length of the deflected top cable. Given that the deflection profile of a cable is related to the deflected cable length, and given that the difference in the deflected cable length between the top and bottom cables was negligible, the deflection profile of the bottom cable was assumed to be the same as that of the top cable in this analysis.

From the cable load and deflection angle time histories, the time history of the reaction force at the four supports was obtained (Fig. A.3), where the peak reaction force is about 4.6 kN. From field measurements of other flow data (Table A.1) at time $T = 7$ s to 8 s when the dynamic peak load occurred, the dynamic debris pressure coefficient α could be estimated at 0.71 to 0.90.

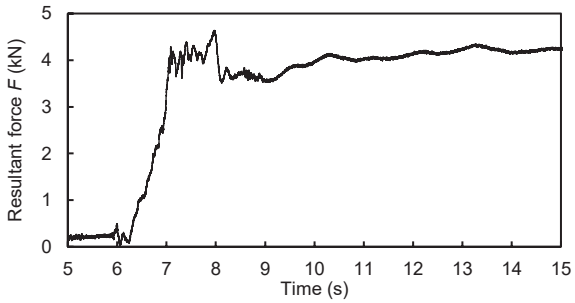

Figure A.3. Time history of total cable reaction force normal to barrier net

Table A.1. Flow data in Test 1 at $T = 7$ to 8 s

Debris density	2000 kg/m^3
Debris velocity	4.6 to 5.2 m/s
Flow width	2 m
Flow depth	60 mm

Appendix B

Documented large-scale debris impact tests on flexible barriers

Case 1 – Illgraben (Wendeler et al., 2008a)

Case 1 involves GeoBrugg's side-anchored flexible barriers installed in Illgraben, Switzerland, where a debris flow occurred in May 2006. The observed flow characteristics and the details of the flexible barrier are given in Tables B.1 and B.2 respectively.

Table B.1. Flow characteristics (Case 1)

Debris depth	Flow velocity	Flow width	Flow density	Debris composition
1 m	2.9 m/s	About 10 m	1600 kg/m^3	Mudflow

The configuration of the flexible debris-resisting barrier system is shown in Figure B.1. The details and load-deformation behaviour of the energy dissipating device were taken from the manufacturer's product manual.

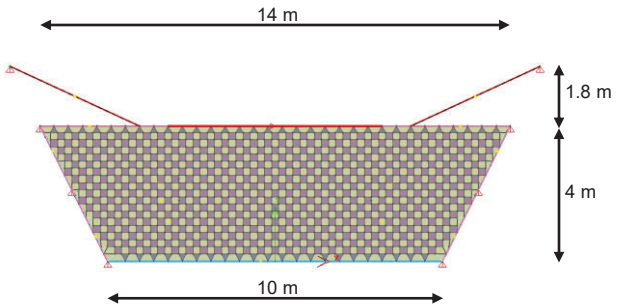

Figure B.1. Modelled barrier (Case 1)

Table B.2. Details of main barrier components (Case 1)

Rope diameter	Ring net	Winglet rope + EDD	Upper rope + EDD	Lower rope + EDD	Intermediate rope + EDD
Geobinex 22 mm	ROCCO 16/3/300	1 rope + 2 GN 9017	2 ropes + 4 GN 9017	2 ropes + 2 GN 9017	8 ropes + 8 GN 9017
Note: EDD = energy dissipating device					

Table B.3. Details of main barrier components (Case 2)

Rope diameter	Wire net	Support rope + EDD	Upslope rope + EDD	Lateral tie rope
Geobinex 22 mm	SPIDER S4-130	1 rope + 2 GN 9017	2 ropes + 2 GN 9017	2 ropes
Note: EDD = energy dissipating device				

Case 2 – Veltheim (WSL, 2011)

Case 2 involves GeoBrugg's post-supported flexible barrier SL-150. The field test was conducted at Veltheim, Switzerland in 2011. The test involved four consecutive releases of 50 m^3 artificially mixed debris flow onto a 40°, 40 m long, 8 m wide flume. Only the first release was modelled. The details of the flexible barrier and the observed flow characteristics are given in Tables B.3 and B.4 respectively.

The configuration of the flexible debris-resisting barrier system is shown in Figure B.2. The details and load-deformation behaviour of the energy dissipating device were taken from the manufacturer's product manual.

Table B.4. Flow characteristics (Case 2)

Debris depth	Flow velocity	Flow width	Flow density	Debris composition by mass
0.5 m	10.2 m/s	8 m	2085 kg/m^3	8% clay 17% silt 30% sand 41% gravel 4% stone Water content 23%

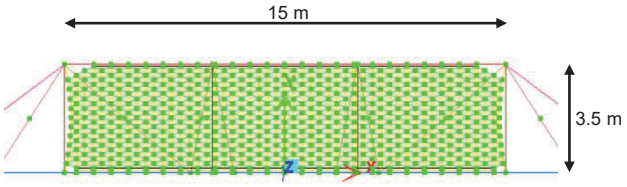

Figure B.2. Modelled barrier (Case 2)

Acknowledgements

The authors are grateful for financial support from the theme-based research grant T22-603/15- N and area of excellence project grant AoE-E603/18, as well as the general research fund grants 16212618, 16209717, and 16210219 provided by the Research Grants Council of the Government of Hong Kong Special Administrative Region, China. S. Poudyal gratefully acknowledges the support of Hong Kong PhD Fellowship provided by the Research Grants Council of Hong Kong.

This paper is published with the permission of the Head of Geotechnical Engineering Office and the Director of Civil Engineering and Development of the Government of the Hong Kong S.A.R.

References

Aquelet, N., Souli, M., and Olovsson, L. (2006). Euler–Lagrange coupling with damping effects: Application to slamming problems. Computer Methods in Applied Mechanics and Engineering, 195(1-3):110–132.

Brown, D. (2016). Tracker: Video Analysis and Modelling Tool. https://physlets.org/tracker/.

Bugnion, L., McArdell, B. W., Bartelt, P., and Wendeler, C. (2012). Measurements of hillslope debris flow impact pressure on obstacles. Landslides, 9(2):179–187.

Chan, S. L., Zhou, Z. H., and Liu, Y. P. (2012). Numerical analysis and design of flexible barriers allowing for sliding nodes and large deflection effects. In Lau, C. K., Chan, E., and Kwan, J. S. H., editors, Proceedings of the One Day Seminar on Natural Terrain Hazards Mitigation Measures, pages 29–43, Hong Kong. Association of Geotechnical and Geoenvironmental Specialists (Hong Kong).

Cheung, A. K. C., Yiu, J., Lam, H. W. K., and Sze, E. H. Y. (2018). Advanced numerical analysis of landslide debris mobility and barrier interaction. HKIE Transactions, 25(2):76–89.

DeNatale, J. S., Iverson, R. M., Major, J. J., LaHusen, R. G., Fiegel, G. L., and Duffy, J. D. (1999). Experimental Testing of Flexible Barriers for Containment of Debris Flows. U.S. Geological Survey Open-File Report 99-205.

EOTA (2013). Guideline for European Technical Approval of Falling Rock Protection Kits. Guideline for European Technical Approval ETAG 027.

EOTA (2016). Flexible kits for retaining debris flows and shallow landslides/open hill debris flows. European Assessment Document EAD 340020-00-0106.

Ferrero, A., Segalini, A., and Umili, G. (2015). Experimental tests for the application of an analytical model for flexible debris flow barrier design. Engineering Geology, 185:33–42.

GEO (2015). Assessment of Landslide Debris Impact Velocity for Design of Debris-resisting Barriers. Geotechnical Engineering Office Technical Guidance Note No. 44.

Iverson, R. M. (1997). The physics of debris flows. Reviews of Geophysics, 35(3):245–296.

Koo, R. C. H. (2017). 3D Debris Mobility Assessment Using LS-DYNA. Geotechnical Engineering Office Report No. 325.

Koo, R. C. H., Kwan, J. S. H., Lam, C., Ng, C. W. W., Yiu, J., Choi, C. E., Ng, A. K. L., Ho, K. K. S., and Pun, W. K. (2017). Dynamic response of flexible rockfall barriers under different loading geometries. Landslides, 14(3):905–916.

Kwan, J. S. H. and Cheung, R. W. M. (2012). Suggestions on design approaches for flexible debris-resisting barriers. Geotechnical Engineering Office Discussion Note No. DN 1/2012.

Kwan, J. S. H., Sze, E. H. Y., and Lam, C. (2019). Finite element analysis for rockfall and debris flow mitigation works. Canadian Geotechnical Journal, 56(9):1225–1250.

Kwan, J. S. H., Sze, E. H. Y., Lam, C., Law, R. P. H., and Koo, R. C. H. (2021). Development and applications of debris mobility models in Hong Kong. Proceedings of the Institution of Civil Engineers - Geotechnical Engineering, 174(5):593–610.

Lam, H. W. K., Sze, E. H. Y., Wong, E. K. L., Choi, C. E., Poudyal, S., and Ng, C. W. W. (2022). Large-scale Debris Impact Test on Flexible Barrier and Back-analysis Using LS-DYNA. In Proceedings of the 3rd International Conference on Natural Hazards and Infrastructure, Athens (in press).

Lam, H. W. K. and Wong, A. L. (2021). Experimental and numerical study of dynamic soil debris impact load on reinforced concrete debris-resisting barriers. Landslides, 18(3):955–966.

Ng, C. W. W. and Choi, C. E. (2019). Final Testing Report (Phase 1), Service Contract for Large-scale Debris Impact Tests on Flexible Barriers. Testing Report prepared for Geotechnical Engineering Office, Hong Kong.

Ng, C. W. W. and Choi, C. E. (2020). Final Testing Report (Phase 2), Service Contract for Large-scale Debris Impact Tests on Flexible Barriers. Testing Report prepared for Geotechnical Engineering Office, Hong Kong.

Ng, C. W. W., Choi, C. E., Liu, H., Poudyal, S., and Kwan, J. S. H. (2021a). Design Recommendations for Single and Dual Debris Flow Barriers with and Without Basal Clearance. In Sassa, K., Mikoš, M., Sassa, S., Bobrowsky, P. T., Takara, K., and Dang, K., editors, Understanding and Reducing Landslide Disaster Risk, volume 1, pages 33–53. Springer International Publishing, Cham. Series Title: ICL Contribution to Landslide Disaster Risk Reduction.

Ng, C. W. W., Choi, C. E., Liu, H., Wang, C., and Kwan, J. S. H. (2021b). Impact mechanisms of debris flow on barriers: modelling, analysis and design. In Cabrera, M., Prada-Sarmiento, L. F., and Montero, J., editors, SCG-XIII International Symposium on Landslides, Cartagena.

Ng, C. W. W., Song, D., Choi, C. E., Koo, R. C. H., and Kwan, J. S. H. (2016). A novel flexible barrier for landslide impact in centrifuge. Géotechnique Letters, 6(3):221–225.

Olovsson, L. and Souli, M. (2000). ALE and fluid-structure interaction capabilities in LS-DYNA. Proceedings of the 6th International

LS-DYNA Conference, 15:37–46.

Song, D., Choi, C. E., Ng, C. C. W., and Zhou, G. G. D. (2018). Geophysical flows impacting a flexible barrier: Effects of solid-fluid interaction. Landslides, 15(1):99–110.

Sze, E. H. Y., Koo, R. C. H., Leung, J. M. Y., and Ho, K. K. S. (2018). Design of flexible barriers against sizeable landslides in Hong Kong. HKIE Transactions, 25(2):115–128.

Tan, D.-Y., Feng, W.-Q., Yin, J.-H., Zhu, Z.-H., and Qin, J.-Q. (2021). Numerical study of retention efficiency of a flexible barrier in mitigating granular flow comparing with large-scale physical modeling test data. Acta Geotechnica, 16(2):433–448.

Tan, D.-Y., Yin, J.-H., Qin, J.-Q., Zhu, Z.-H., and Feng, W.-Q. (2020). Experimental study on impact and deposition behaviours of multiple surges of channelized debris flow on a flexible barrier. Landslides, 17(7):1577–1589.

Volkwein, A. (2014). Flexible debris flow barriers – design and application. WSL Ber, (18).

Wendeler, C. (2008). Field investigations and modeling of the interaction of debris flows with flexible ring-net barriers. Doctoral dissertation, ETH Zurich, Switzerland.

Wendeler, C., McArdell, B. W., Volkwein, A., Denk, M., and Gröner, E. (2008a). Debris flow mitigation with flexible ring net barriers – field tests and case studies. In Monitoring, Simulation, Prevention and Remediation of Dense and Debris Flows II, pages 23 – 31. WIT Press.

Wendeler, C., Volkwein, A., McArdell, B. W., and Bartelt, P. (2019). Load model for designing flexible steel barriers for debris flow mitigation. Canadian Geotechnical Journal, 56(6):893–910.

Wendeler, C., Volkwein, A., Roth, A., Herzog, B., Hählen, N., and Wenger, M. (2008b). Hazard prevention using flexible multi-level debris flow barriers. Protection against debris flows by installation of 13 flexible barriers in the Milibach River (Canton Berne, Switzerland). In Mikos, M., Huebl, J., and Koboltschnig, G., editors, INTERPRAEVENT 2008: Protection of populated territories from floods, debris flow, mass movements, and avalanches, volume 1, pages 547–554, Dornbirn, Vorarlberg, Austria.

Won, S., Lee, S. W., Paik, J., Yune, C.-Y., and Kim, G. (2016). Analysis of Erosion in Debris Flow Experiment Using Terrestrial LiDAR. Journal of the Korean Society of Surveying, Geodesy, Photogrammetry and Cartography, 34(3):309–317.

WSL (2011). Report on Testing SL-150 a Protection System against Shallow Landslides. Test Report No. 10-17, WSL, Switzerland.

Xiao, S., Su, L., Jiang, Y., Qu, X., Xu, M., Hu, X., and Liu, Z. (2020). Experimental investigation on the impact force of the dry granular flow against a flexible barrier. Landslides, 17(6):1465–1483.

Zhang, B., Huang, Y., and Liu, J. (2021). Micro-mechanism and efficiency of baffle structure in deceleration of granular flows. Acta Geotechnica, 16(6):1–22.